encit 2020

18th Brazilian Congress of Thermal Sciences and Engineering
November 16-20, 2020 (Online)

ENC-2020-0358
EXPERIMENTAL EVALUATION OF THE FLOW BOILING HEAT TRANSFER COEFFICIENT OF R600A AND R134A INSIDE A 9.43 MM INNER DIAMETER TUBE.

Guilherme Henrique de Sena e Oliveira, guilherme.sena.oliveira@usp.br[1]
Tiago Augusto Moreira, tiago.moreira@usp.br[1]
Gherhardt Ribatski, ribatski@sc.usp.br[1]

[1]*Heat Transfer Research Group – HTRG*, Departamento de Engenharia Mecânica, Escola de Engenharia de São Carlos (EESC), University of São Paulo (USP), Av. Trabalhador São-Carlense, 400, Parque Arnold Schimidt, CEP: 13566-590, São Carlos, Brasil.

Abstract. *This paper concerns an experimental investigation of the heat transfer coefficient during flow boiling of R134a and R600a inside a horizontal smooth circular tube with inner diameter of 9.43 mm. Experiments were performed for mass velocities ranging from 100 to 200 kg/m^{2}s, heat fluxes from 10 to 30 kW/m^2, vapor qualities up to the unity, and saturation temperature of 5^{o}C. Generally, an increase of the heat transfer coefficient was observed with increasing heat flux and mass velocity. The heat transfer coefficient increases with increasing vapor quality until dryout conditions are reached. Any additional vapor quality increment beyond dryout causes a decrease in the heat transfer coefficient. In general, higher heat transfer coefficients were noticed for R600a compared to R134a under similar experimental conditions. Unsatisfactory predictions were provided for both fluids by the prediction methods from literature at high vapor qualities corresponding to conditions close to the surface dryout, while predictions for lower vapor qualities performed better.*

Keywords: *Flow boiling, heat transfer coefficient, two-phase flow, R134a, R600a.*

1. INTRODUCTION

Recently, because environmental concerns such as global warming and ozone layer depletion, a demand for environmental-friendly refrigerants was propelled based on the Montreal protocol and the Kigali amendment (Moreira et al., 2021). Among those fluids, hydrocarbons (HCs) have drawn attention because of their low global warming potential (GWP) and null ozone layer depletion potential (ODP). However, due to their flammability, an optimization of the refrigeration systems focusing on reducing the refrigerant charge is necessary to increase their range of applicability obeying the safety protocols. As pointed out by Moreira et al. (2021), most of the mass in refrigeration systems is concentrated in the heat exchangers, therefore, they should be the main focus of optimization concerning the reduction of the overall refrigerant charge. For it, robust and accurate prediction methods for the heat transfer coefficient, which relays on experimental data, are necessary.

Shin et al. (1996), Lee et al. (2005), and Qiu et al. (2016) found higher heat transfer coefficients for R600a compared to halocarbons and HFOs in their experimental studies. In general, these authors attributed such results to the lower viscosity and higher thermal conductivity of hydrocarbons compared to halocarbons and HFOs. This implies on high turbulence effects and the reduction of the thermal resistance associated to the conduction through the liquid film in annular flows. Lee et al. (2005) compared their data against the prediction methods of Shah (1982), Gungor and Winterton (1986), and Kandlikar (1990), founding reasonable agreement for the method of Kandlikar (1990).

Although the number of flow boiling experimental studies involving the heat transfer coefficient of R600a has been increasing over the past few years, they are still scarce, covering a restricted range of experimental conditions, as pointed out in the recently broad literature review performed by Moreira et al.

(2021). In this context, the current study presents results for the flow boiling heat transfer coefficient of R600a and R134a inside a horizontal smooth tube. The data gathered during the experiments are compared against prediction methods, and the accuracies of these methods are assessed.

2. EXPERIMENTAL SETUP

The experimental apparatus is comprised of two water-heating circuits, one for the test section and another for the pre-heater, a water-glycol cooling circuit for the sub-cooler and the condenser, and a refrigerant circuit (also named as main circuit), schematically shown in Fig. 1. In this paper, only the main loop is detailed. In this circuit, the fluid from the condenser is driven through the test loop by one of two magnetic gear pumps, A for high mass fluxes (micropump GD 223/56C), and B for low mass fluxes (micropump GC M23 JKS5). Downstream the pumps, the fluid flows through a Coriolis mass flow meter (TRIRCOR TCM-5500) and then, through the sub-cooler, where heat is rejected to a mixture of water and ethylene-glycol. The sub-cooler is used to ensure subcooled liquid at the inlet of the pre-heater, at which the temperature and pressure (using a Danfoss transducer 060G3043, range from 0 to 2500 kPa) of the fluid are measured to determine its enthalpy. At the outlet of the pre-heater pressure (Danfoss transducer 060G3043, range from 0 to 2500 kPa) and temperature of the working fluid are also measured. The pre-heater heater consists of an 8 meters length counter-current heat exchanger, with hot water flowing in the annuli and the working fluid in the inner tube. The pre-heater outer tube is made of chlorinated polyvinyl chloride and the inner of stainless-steel. Water temperatures are measured at the inlet and outlet of this heat exchanger, and its volumetric flow rate is measured by an electro-magnetic volumetric flow meter (Rosemount, 8711) positioned downstream the pre-heater. To obtain the water mass flow rate, the volumetric flow rate is multiplied by the density of the water evaluated based on the measured temperature at the outlet of the pre-heater. Downstream the pre-heater the fluid flows through a 2 m long stabilization section, to ensure full hydraulic development for the flow at the inlet of the test section.

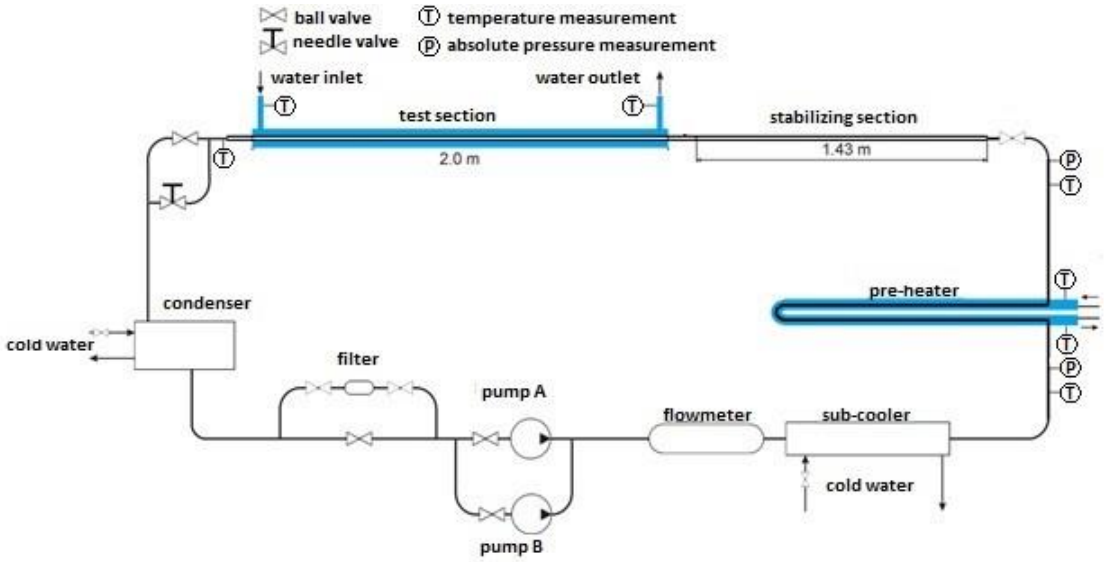

Figure 1. Schematic of the main (refrigerant) circuit.

The test section, schematically illustrated in Fig. 2, consists of a tube-in-tube heat exchanger, with the working fluid flowing inside the inner tube (9.43 mm ID and 13.6 mm OD), and water flowing counter-currently in the annuli (outer tube ID of 18 mm). For water temperature measurements at the inlet and outlet of the test section two thermistors from FLUKE Corp. (CSP60BA103M-H/2-90 4-wire) with high accuracy (smaller than 0.01°C when their resistance is measured) are used. In order to keep their accuracy, two precision multimeters, TEKTRONIX DMM4020 for water inlet, and TEKTRONIX DMM4040 for water outlet, are used to measure the thermistors resistance and calculate the temperature through the equations given by the manufacturer (FLUKE Corp.). Four equally spaced temperature measurement sections are distributed along the test section. A schematic view of the cross sections displaying the thermocouples arrangement is shown in Fig. 2. In each section, there are four thermocouples placed within the water flow, one placed inside a hole in the inner tube (1.7 mm depth) to measure the wall temperature, and one placed inside a bulb within the inner tube to measure the

temperature of the working fluid. At the inlet and outlet of the test section, there are three differential pressure transducers from Endress-Hauser (ranges of 0-3, 0-10 and 0-300 kPa) used to measure the pressure drop along its length. At the test section inlet, an absolute pressure transducer (Danfoss 060G3043, range from 0 to 2500 kPa) is connected to evaluate the local pressure. To obtain the water mass flow rate, the volumetric flow rate evaluated through an electro-magnetic volumetric flow meter (Rosemount, 8711) is multiplied by the density of the water obtained based on its temperature at the outlet of the test section. The test section is insulated with a 50 mm thick layer of mineral wool, covered by a 20 mm layer of elastomeric foam.

Downstream the test section, there is a T-junction, with in one side a needle valve and in the other a ball valve. The use of the needle valve is necessary at low mass fluxes to control the pressure inside the test section. Closing the circuit, the fluid returns to the condenser, a shell-and-tube heat exchanger, at which the refrigerant is condensed at the shell side using the water/ethylene-glycol circuit flowing in the tubes side. Along the loop, except by the thermistors, all temperatures are measured through K-type thermocouples with hot junction diameter of 0.254 mm from Omega Inc. To record the data, and monitor, and control the experimental apparatus, a National Instruments data acquisition system (chassis SCXI-1000 associated to the modules SCXI-1303, SCXI-1302 and SCXI-1112) with a LabView (2013) program were used.

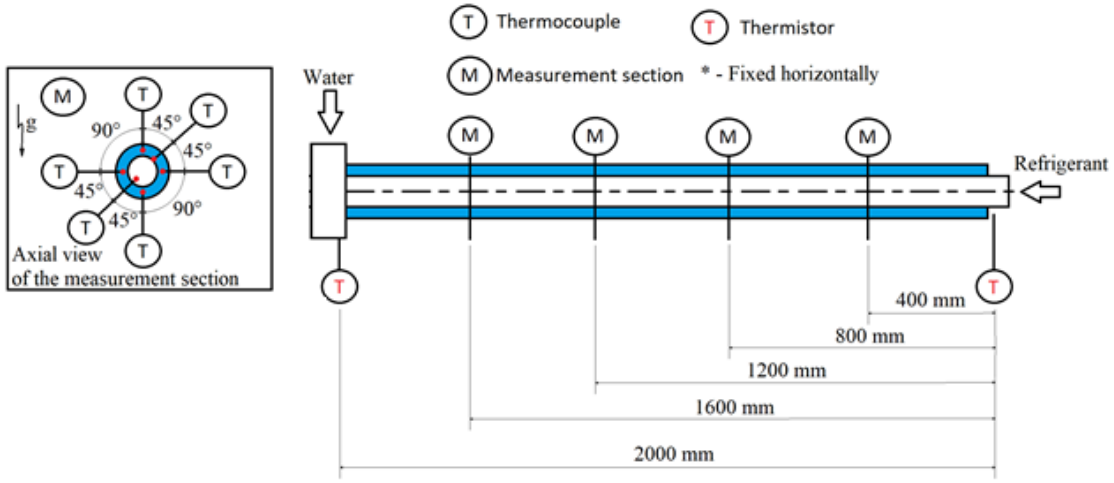

Figure 2. Schematic of the test section.

2.2 Data regression procedure

Data reduction was performed using the Matlab (2015a) software. Fluid properties were obtained from Coolprop (Bell et al., 2014). For the measurements, the test section length was divided in five discrete elements according to lengths showed in Fig. 2.. Therefore, considering the inlet and outlet of the test section, the discretization index i varies from 1 (refrigerant-side inlet and water-side outlet) to 6 (refrigerant-side outlet and water-side inlet).

The mass velocity, G, was calculated as the ratio between the mass flow rate measured through the Coriolis mass flow meter and the internal cross sectional area of the test section.

The heat transfer coefficient was estimated according to the Newton's cooling law as follows:

$$h = \frac{q''_i}{T_{w,i} - T_{fi}} \tag{1}$$

where q''_i is the local heat flux, T_{fi} the local fluid temperature, and $T_{w,i}$ the wall temperature at the inner surface of test tube. $T_{w,i}$ is estimated through the Fourier's law considering unidimensional conduction between the location of the thermocouple, T_{read}, and the innertube surface, as follows:

$$T_{w,i} = T_{read} - \frac{\left(\frac{\ln(d_e - 2e_h)}{d_{int}}\right)}{2k_{tube}} q'' \tag{2}$$

where d_{int} is the internal diameter, and d_e is the external diameter of the test tube, e_h is the depthness of the hole in which the wall thermocouple is placed, and $k_{tube}$is the thermal conductivity of the tube.

The value of q''_i is estimated by a discrete local energy balance, as follows:

$$q''_i = \frac{\dot{m}_{water} c_{p,water}}{\pi d_{int}} \left(\frac{dT_{water}}{dz_i}\right) - \frac{Q_{losses}}{d_{int} \pi L_{section}} \tag{3}$$

where, $\dot{m}_{water}$ is the water mass flow rate, $c_{p,water}$ the specific heat of the water, $T_{i,water}$ the water temperature at the measurement section (arithmetic average of the measurements given by the four thermocouples, see Fig. 2) and z_i the axial distance from the inlet of the test section. Q_{losses} is the heat losses to the ambient, which temperature is controlled to be at 19°C, between each measurement section. $L_{section}$ is the length between the measurement sections. To estimate Q_{losses}, tests were performed by flowing water at 15, 20, 25, 30 and 35°C and mass flow rates of 0.16 and 0.08 kg/s in the annuli and with vacuum inside the inner tube of the test section. Based on the temperature difference between the inlet and outlet of the water, heat losses (or gains, depending on the water temperature) were estimated and correlated as a function of the temperature difference between the water and the environment. A similar procedure was adopted for the pre-heater.

The term $\frac{dT_{water}}{dz_i}$ is the derivative of the water temperature profile along the test section length. The water temperature profile was adjusted as a second-degree polynomial based on the water temperature measurements, see Fig. 2, using the weighted least squares method, similarly to the procedure adopted by Del Col et al. (2011).

The local vapor quality is estimated through the following equation:

$$x_{local} = \frac{i_i - i_l}{i_{lv}} \tag{4}$$

where i_{lv} is the vaporization enthalpy, and i_l the saturated liquid enthalpy of the working fluid at the local pressure of the flow, estimated as follows:

$$P_i = \Delta P \frac{L_i}{L} \tag{5}$$

where L_i is the distance between the measurement sections and the test section inlet, L is the total length of the test section, and ΔP is the total pressure drop measured by the differential pressure transducers. The local enthalpy of the fluid, i_i,, an energy balance was performed between the fluid and the water in the annuli at each measurement secton as follows:

$$i_i = i_{i-1} + \frac{\left(\dot{m}_{water}\left(T_{water,i} - T_{water,i-1}\right) - Q_{losses}\right)}{\dot{m}_{fluid}} \frac{L_i}{d_{int}\pi} \tag{6}$$

where i_{i-1} is the enthalpy of the fluid in the previous discrete element inlet considering the refrigerant flow direction, and $\dot{m}_{fluid}$ the mass flow rate of the working fluid.

2.3 Calibration procedures and uncertainty analysis

Temperature measurements performed by thermocouples along the loop (except by the ones at the test section) were calibrated using a thermal bath (Haake AC200-A40) associated with a precision thermometer (FLUKE-1523-P1 reference thermometer, probe 5616 PRT, uncertainty of 0.011°C). For the thermocouples placed at the test section, the calibration was made *in loco*, with water flowing in the annuli and vacuum inside the test tube. To control the temperature of water, the same thermal bath above mentioned was used, with a centrifugal pump (Mark NXDP-2, 0.5 cv) being responsible for flowing the water in the annuli at high Reynolds numbers. In this case, the reference temperature was assumed as the average between the thermistors placed at the inlet and outlet of the test section (0.02°C maximum difference between the temperature read by the thermistors+multimeters pairs). In both thermocouples

calibration setups, the uncertainties were evaluated according to the procedure suggested by Abernethy and Thompson (1973)

The absolute and differential pressure transducers were calibrated using a manual pump and a pressure indicator from WIKA Co., model CPG 2500 (0-2000kPa, accuracy of 0.08 kPa), with the uncertainty evaluated also by the method of Abernethy and Thompson (1973). The uncertainty of the measurements provided by the manufacturer were adopted for the magnetic flow meters, Coriolis mass flow meter and the thermistors. The uncertainty propagation procedure presented by Taylor and Kuyatt (1994) was used to estimate the heat transfer coefficient uncertainty. In general, its uncertainties presented a mean value of 6.3% and always lower than 10%. The uncertainties for the measured and calculated parameters are displayed in Tab. 1. The procedure by Taylor and Kuyatt (1994) was also used to obtain the uncertainty of the heat flux and vapor quality. For the heat flux, the mean value found is 2.1%, and the maximum is 3.6%. For the vapor quality, the mean value found is 0.02, and the maximum is 0.03.

Table 1. Experimental uncertainties.

Measurement	**Uncertainty**
Temperature (thermistors)	0.005°C
Temperature (thermocouples)	0.025°C
Absolute pressure	0.08 kPa
Differential pressure	0.075% of full scale
Refrigerant mass flow rate	0.1%
Water volumetric flow rate	0.25%
Tube diameter	0.1 mm
Heat flux	2.1%
Heat transfer coefficient	6.3%
Vapor quality	0.02

Single-phase tests were performed for R134a to validate the experimental facility and data regression procedures. The results for heat transfer coefficient found were compared with predictions obtained through Gnielinski (1976). A mean absolute deviation of 5.3% was found. This result can be considered satisfactory to validate the experimental apparatus and data regression procedures.

3. EXPERIMENTAL RESULTS

Flow boiling experiments were performed for R134a and R600a at a saturation temperature of 5±1°C, mass velocities ranging from 100 to 200 kg/m^{2}s and heat fluxes from 10 to 30 kW/m^2. As shown in Figs. 3, 4, 5 and 6, higher heat transfer coefficients were obtained for R600a compared to R134a, with the difference among the results reaching a maximum at intermediary vapor qualities (x≈0.65). It is speculated that the main reasons why the R600a overperformed R134a is its higher thermal conductivity.

The comparison of Figs 3 to 6 shows that the heat transfer coefficient increases with increasing mass velocity and heat flux for both fluids. For q''=10 kW/m^2, (Figs. 3 and 4) different behaviors are noticed for R134a and R600a previously the onset of dryout, i. e. steep drop in the heat transfer coefficient with increments in quality. For R600a, the heat transfer behaves as dominated by shear effects, with the heat transfer coefficient increasing with increments in quality until dryout incipience. For R134a, the heat transfer is dominated by nucleate boiling effects since vapor quality has a practically null effect on the heat transfer coefficient up to the incipience of dryout. Such difference is related to the difference among fluid properties, mainly the specific volume of the vapor-phase, v_v, as displayed in Tab. 2. Because R600a presents a much larger v_v, around 3 times greater than R134a, under similar conditions of x and G it presents a higher flow velocities, suppressing bubble nucleation and leading the heat transfer to be dominated by convective effects.

For q=30 kW/m^2 and G=100 kg/m^{2}s (Fig. 5), the qualitative heat transfer behaviors are almost similar than those observed for q=10 kW/m^2, however, smaller differences between the heat transfer coefficients of the fluids are displayed. Such result is related to the fact that increments in heat flux provides a larger increment of the heat transfer coefficient for R134a compared to R600a. This behavior is associated to the predominance of nucleate boiling effects for R134a, while convective effects prevails for R600a. As pointed out by Kandlikar (1990) and Kandlidar and Steinke (2002), the main factors that determine whether convective or nucleate boiling effects are dominant in the heat transfer are the ratio between the densities of vapor and liquid phases (ρ_l/ρ_v) and the boiling number (Bo). The ratio between phases

density determine the difference in the velocities of the phases. For a smaller ratio, the difference between velocities is higher, and so the shear stress in the interface is higher, which increases convective effects and suppresses bubble nucleation. The boiling number is directly related to nucleate boiling effects, being defined as the ratio among heat flux and flow heat capacity (mass velocity multiplied by the enthalpy of vaporization of the fluid, i_{lv}), as follows:

$$Bo = \frac{q''}{i_{lv}G} \tag{7}$$

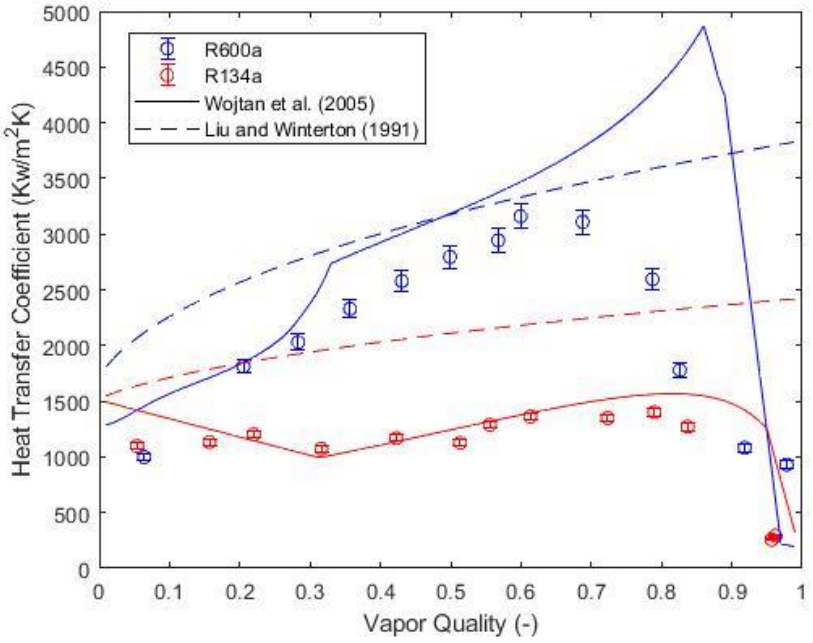

Figure 3. Comparison between experimental results for the heat transfer coefficient at $G = 100$ kg/m^{2}s, $q'' = 10$ kW/m^2, $T_{sat} = 5$°C.

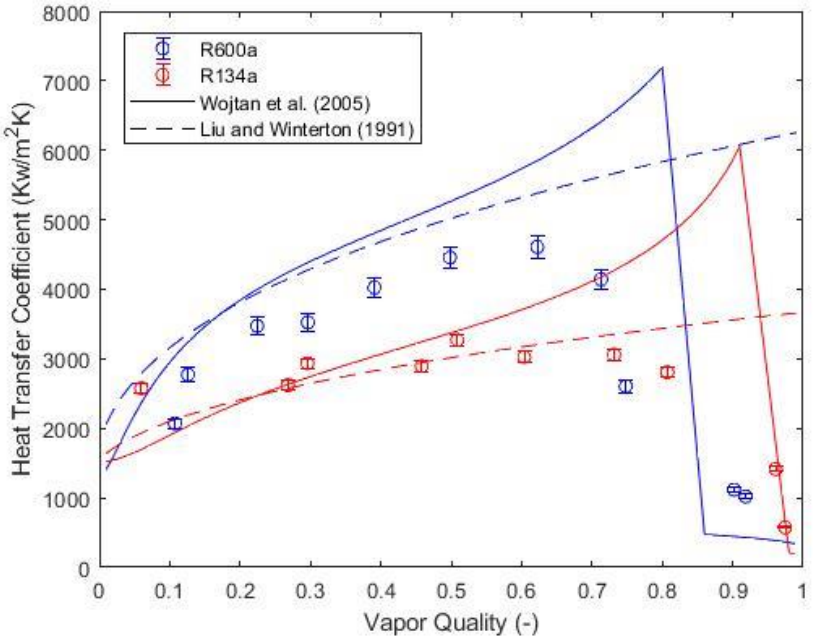

Figure 4. Comparison of experimental results for heat transfer coefficient at $G = 200$ kg/m^{2}s, $q'' = 10$ kW/m^2, $T_{sat} = 5$°C.

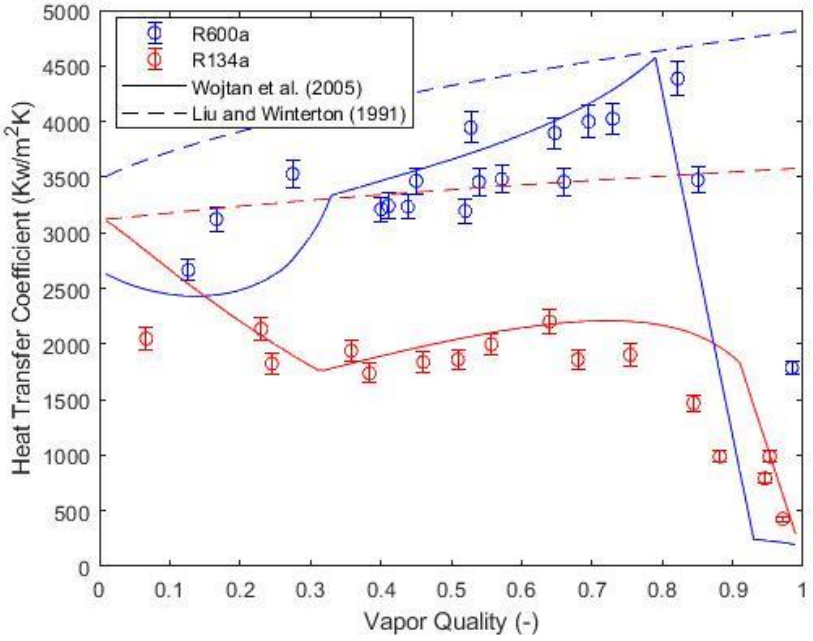

Figure 5. Comparison of experimental results for heat transfer coefficient at $G = 100$ kg/m^{2}s, $q'' = 30$ kW/m^2, $T_{sat} = 5^oC$.

As displayed in Tab. 2, under the conditions evaluated in the present study, R134a presents a higher boiling number, while the R600a presents a lower ρ_l/ρ_v. Such results corroborate the previous hypothesis that considers nucleate boiling effects dominant for R134a for and convective effects for R600a.

Table 2. Values for specific volume of the vapor phase, rate between phases density and boiling number for both fluids at T=5°C.

Fluid	v_v **(m^3/kg)**	ρ_l/ρ_v **(-)**	Bo (10^{-4}) $G = 100\ kg/m^2s$ q''**=(10/30 kW/m^2)**	Bo (10^{-4}) $G = 200\ kgm^2s$ q''**=(10/30 kW/m^2)**
R600a	0.19	114.6	(2.86/8.58)	(1.43/4.29)
R134a	0.06	74.6	(5.14/15.40)	(2.57/7.70)

For q''=30 kW/m^2 and G=200 kg/m^{2}s (Fig. 6) the heat transfer behavior of R600a remains the same, however, a change in the slope of the curve of h with increasing quality is noticed for R134a. According to Fig. 6, the heat transfer coefficient for R134a initially increases with increasing quality, until it reaches a maximum around x≈0.5, from which any increment in quality causes a reduction of the h, in which condition, the presence of a liquid film was still verified. Such behavior is kept until x≈0.8, from which the decrease of the heat transfer coefficient with increasing vapor quality becomes steeper, characterizing the incipience of dryout. It is speculated here that the change in the slope of the heat transfer coefficient for R134a is related to a suppression of nucleate boiling effects caused by the increase in flow velocity as x rises.

Figures 3 and 4 reveal an earlier incipience of dryout in terms of vapor quality for R600a, x_{di}≈0.62, compared to R134a, x_{di}≈0.81.This behavior is related to the lower density of the vapor-phase for R600a, see Tab. 2, which causes a higher shear stress on the liquid-vapor interface, increasing the entrainment rate and, consequently, reducing the liquid film thickness and anticipating in terms of vapor quality the formation of the first dry-patches. The lower viscosity of R600a corroborates to this behavior because it implies on thinner liquid films during annular flow, thus causing the dryout to occur at lower qualities compared to R134a. In Figs. 5 and 6, the dryout incipience vapor quality of the fluids is closer. This is related to the higher density of bubbles nucleation expected with increasing heat flux for R134a. It can be speculated that the higher tendency for bubble nucleation favors the appearance of dryout regions near the wall, thus reducing the dryout incipience.

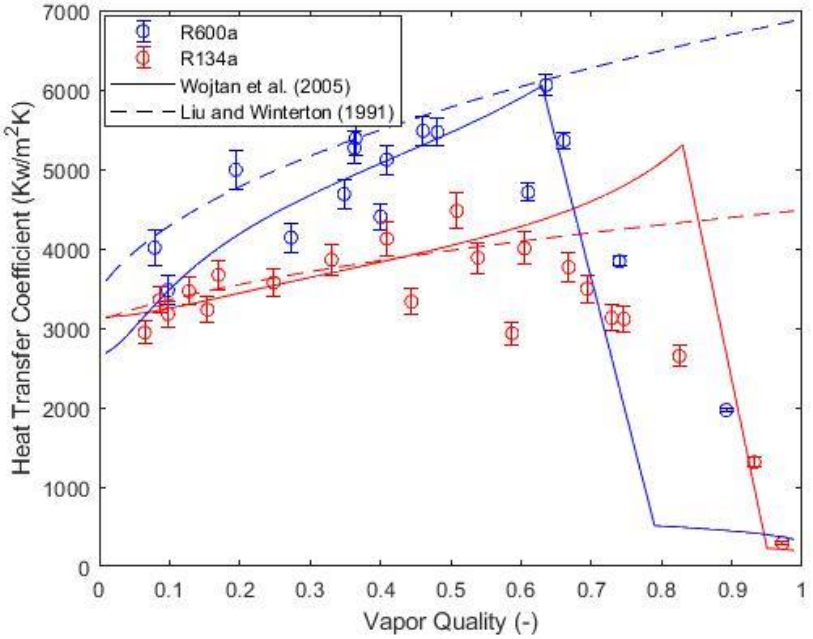

Figure 6. Comparison of experimental results for heat transfer coefficient at $G = 200$ kg/m^{2}s, $q'' = 30$ kW/m^2, $T_{sat} = 5^{o}$C.

4. ASSESSMENT OF PREDICTION METHODS ACCURACY

Table 3 shows the results of a comparison between the data obtained in the present study and prediction methods from literature. The statistical parameters used to assess the accuracy of prediction methods were the mean absolute error (MAE) and the percentage of predictions within a ±20% error band. In both cases, the best predictions were obtained by the method of Wojtan et al. (2005), which showed for R600a MAE=41.9%, predicting 41.2% within an error band of ±20%. For R134a, better results were also found with the method of Wojtan et al. (2005) showing a mean absolute error of 56.4%, predicting 63.2% of the data within a ±20% error range. As illustrated in Tab. 3, the other methods provided much less accurate predictions of the present database compared to the method of Wojtan (2005). Such results are attributed here to the fact that, among the methods in Tab. 3, only Wojtan et al. (2005) presents an specific modeling for the dryout region, which composes 33.3% of the data for R134a and 23.3% of the data for R600a.

Table 3. Results of comparison between experimental data and predictions (MAE(%) / percentage within 20% error)

Method:	**R600a**	**R134a**
Chen et al. (1966)	238.5/22.6	252.0/32.4
Gungor and Winterton (1986)	273.5/28.0	242.2/26.3
Kandlikar (1990)	247.2/9.0	566.6/7.0
Liu and Winterton (1991)	58.9/41.2	114.6/35.3
Wojtan et al. (2005)	41.9/36.4	56.4/63.2

Figure 7 shows a box-plot illustrating the distribution of absolute errors for the prediction method by Wojtan et al. (2005). The data is ordered and divided into four quarters, having 25% of the data in each and the red line corresponds to the median of the database. The points above or below the third and fourth quarters are statistically considered discrepancies. Fig. 7a shows that most of the predictions made by Wojtan et al. (2005) underestimated the experimental results for R600a, while Fig. 7b shows that most of the data for R134a are over-estimated, since the median is below 0 for the R600a and above 0 for the R134a. In both cases there were found many discrepancies, which are the main reason for the elevate MAE noticed in in Tab. 3. The reason for this is that the method often under or over-predicts the values for the dryout incipience quality.

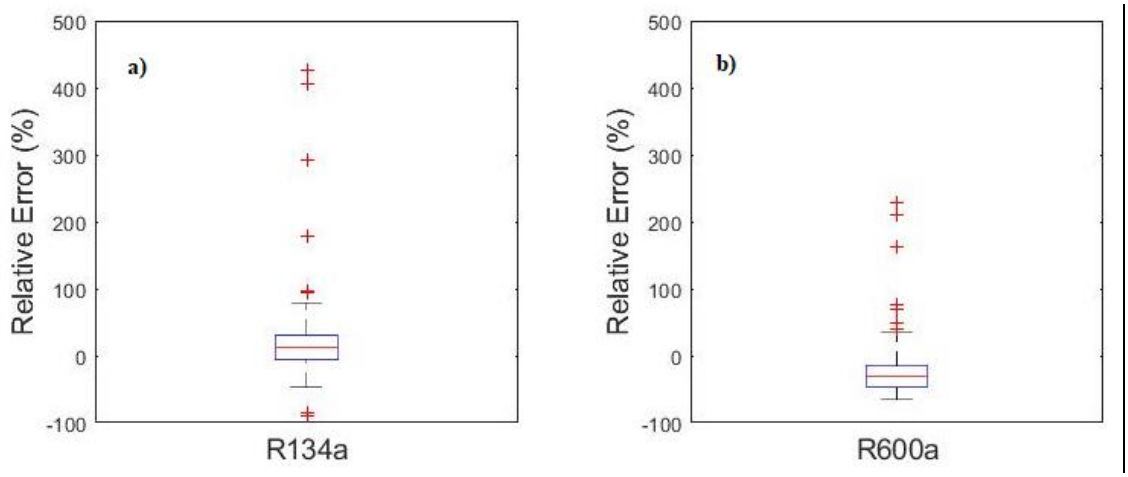

Figure 7. Relative errors obtained between the R134a (a) and R600a (b) data and predictions made by the method of Wojtan et al. (2005).

5. CONCLUSIONS

The results obtained in the present study reveals that R600a presents higher flow boiling heat transfer coefficients than R134a under similar experimental conditions prior the incipience of dryout. However, the hydrocarbon provides a dryout incipience at lower vapor qualities.

In general, a different behavior with varying quality was found for R600a and R134a. In the first, a dominance of convective effects was noticed, with the heat transfer coefficient increasing with increments in quality. For R134a, the flow boiling heat transfer coefficient behavior indicates that nucleate boiling effects are dominant, i. e. negligible effect of varying quality for $x<x_{di}$

In general, the prediction methods evaluated in this study fail into predict accurately the experimental data obtained in the present study. This is likely related to the fact that most of these methods were developed for pre-dryout conditions, which corresponds to only a fraction of the data obtained of this study (71.7% of the database). The predicted values for the heat transfer coefficient for vapor qualities higher than the one corresponding to the dryout incipience are usually close to the ones prior to the dryout, while according to the experimental data the heat transfer coefficient decreases abruptly for $x>x_{di}$. This implies on absolute deviations between predictions and experimental data considerably elevate under dryout conditions, which causes high overall MAE results. Despite the inaccurate predictions, the best results for both fluids were provided by Wojtan et al. (2005), which models the post-dryout condition.

6. ACKNOWLEDGEMENTS

The authors acknowledge the CNPq (National Council for Scientific and Technological Development, Brazil) for the grant given under Contract Number 305673/2017-3, and FAPESP (São Paulo Research Foundation, Brazil) for the scholarships under Contract Numbers 2016/16849-3 and 2018/06057-4. Also, this study was financed in part by the Coordenação de Aperfeiçoamento de Pessoal de Nível Superior - Brasil (CAPES) - Finance Code 001.

7. REFERENCES

Abernethy, M. A., & Guthrie, C. H. (1994). “An empirical assessment of the “fits" between strategy and management information system design” .*Accounting and Finance*, Vol. 34, pp.49-66.

Bell, H. I., Wronski, J., Quoilin,S. Lemort, V. (2014). “Pure and Pseudo-pure Fluid Thermophysical Property Evaluation and the Open-Source Thermophysical Property Library CoolProp”. *Industrial and Engeneering Chemistry Research*, Vol. 53, No. 6, pp. 2498-2508.

Chen, C. J. (1966). “Correlation for boiling heat”. *Industrial & engineering chemistry process design and development , Vol.3*, pp. 322-329.

Del Col, D., Bortolin, S., Cavallini, A., Matkovic, M., (2011). “Effect of cross sectional shape during condensation in a single square minichannel”. *International Journal Heat and Mass Transfer*, Vol. 54, pp. 3909–3920.

Gnielinski, V. (1976). “New equations for heat and mass transfer in turbulent pipe and channel flow”, *International Chemistry Engeneering*, Vol. 16 pp. 359–367

Gungor, K. E.; H, W. R. S. “A general correlation for flow boiling in tubes and annuli”. *International Journal of Heat and Mass Transfer*, Birmingham, Vol. 29, No. 3, pp. 351-358.

Kandlikar, S. G. (1990). “A General Correlation for Saturated Two-Phase Flow Boiling Heat Transfer Inside Horizontal and Vertical Tubes”. *Journal of Heat Transfer* ,Vol. 112 , pp. 219-228.

Kandlikar, S. G. (1991). “Development of a Flow Boiling Map for Subcooled and Saturated Flow Boiling of Different Fluids Inside Circular Tubes”. *J. Heat Transfer* ,Vol. 113, pp. 190-200.

Kandlikar, S. G., & Steinke, M. E. (2002). “Flow Boiling Heat Transfer Coefficient In Minichannels − Correlation and Trends”. *Proceeding of International Heat Transfer Conference* 12.

Liu, Z., & Winterton, R. H. (1991). “A general correlation for saturated and subcooled flow boiling in tubes and annuli, based on a nucleate pool boiling equation”. *International Journal of Heat and Mass Transfer* , Vol. 34 , pp. 2759-2766

MATLAB 2015a, 2015. The Mathworks. Inc., Natick- MA, USA .

Moreira, T. A., Furlan, G., Oliveira, G. H . S., Ribatski, G. (2021). “Flow boiling and convective condensation of hydrocarbons: A state-of-the-art literature review”. *Applied Thermal Engineering*, vol. 182, p. 116129.

Nasr, M., Akhavan-Behabadi, M. A., Momenifar, M. R., Hanafizadeh, P. “Heat transfer characteristic of R-600a during flow boiling inside horizontal plain tube”. *International Communications in Heat and Mass Transfer*, Vol. 66, pp. 93-99.

National Instruments, software LabView, (2013).

Qiu, J. et al. “Experimental investigation of flow boiling heat transfer and pressure drops characteristic of R1234ze(E), R600a, and a mixture of R1234ze(E)/R32 in a horizontal smooth tube”. *Advances in Mechanical Engineering***,** Vol.7, pp.1-12.

Shin, J. Y.; KIM, M. S.; RO, S. T. (1997) Experimental study on forced convective boiling heat transfer of pure refrigerants and refrigerant mixtures in a horizontal tube. *International Journal of Refrigeration*, Vol. 20, n. 4, pp. 267-275.

Taylor, B. N., & Kuyatt, C. E. .(1994) *“Guidelines for evaluating and expressing the uncertainty of NIST measurement results”*, NIST Technical Note 1297, 1994 edition.

Wojtan, L., Ursenbacher, L., Thome, J. R. (2005).” Investigation of flow boiling in horizontal tubes: Part II—Development of a new heat transfer model for stratified-wavy, dryout and mist flow regimes”. *International Journal of Heat and Mass Transfer*, Vol.48, pp.2970-2985.

Yang, Z., Gong, M., Chen, G., Zou, X. Shen, J. “Two-phase flow patterns, heat transfer and pressure drop characteristics of R600a during flow boiling inside a horizontal tube”. *Applied Thermal Engineering*, Vol.120, pp.654-671.

8. RESPONSIBILITY NOTICE

The authors are the only responsible for the printed material included in this paper.